


Universal intrinsic higher-rank spin tensor Hall effect

Ying Su,^{*} Junpeng Hou,^{*} and Chuanwei Zhang[†]

Department of Physics, The University of Texas at Dallas, Richardson, Texas 75080-3021, USA

 (Received 18 January 2021; revised 3 January 2023; accepted 30 January 2023; published 10 February 2023)

The spin Hall effect with nonzero transverse spin current but vanishing charge current has important applications in spintronics. Owing to the half-spin nature of electrons, the spin transport has hitherto been restricted to the rank-1 spin vector, whereas higher-rank spin tensors exist and play important roles in larger-spin (≥ 1) systems. For instance, there are five linearly independent rank-2 spin quadrupole tensors, characterizing the spin nematics, in a spin-1 system. While these internal spin-tensor degrees of freedom substantially enrich the quantum phases and dynamics of large-spin ultracold gases, the quantum transport of spin tensors remains largely unexplored yet. Here we investigate the higher-rank spin tensor current and introduce the concept of the spin tensor Hall effect (STHE) in a large-spin system. We find that a net transverse spin tensor current can be driven by an external field in the longitudinal direction, while no lower-rank spin or charge current exists. Significantly, we identify a universal rank-2 spin tensor Hall conductivity $q/8\pi$ (with the carrier charge q) in a spin-1 model with intrinsic spin-orbit coupling, which is independent of the detailed model parameters. The STHE requires the violation of time-reversal symmetry (TRS) but can be protected by a unique pseudo-TRS associated with the rank-2 spin tensor. An experimental scheme is proposed to realize and detect the STHE with pseudospin-1 ultracold fermionic atoms and through the spin tensor accumulation. A general route towards the generalization of the STHE for larger spins is provided, using the $SU(2)$ subalgebra and generalized Gell-Mann matrix representation of the $SU(N)$ group. Our work reveals an intrinsic spin tensor transport phenomenon and introduce a new member to the Hall effect families, which may pave the way to spin-tensor-tronics.

DOI: [10.1103/PhysRevB.107.085410](https://doi.org/10.1103/PhysRevB.107.085410)

I. INTRODUCTION

Hall effects and their quantized siblings are one of the major cornerstones of modern condensed matter physics, and the discovery of novel Hall effects often opens new avenues for controlling electronic transport for device applications. One of the most notable examples in this context is probably the spin Hall effect (SHE), where spin up and down electrons are deflected to opposite transverse directions under an applied electric field, yielding a nonzero spin current but vanishing charge current [1,2]. Spin-current-based phenomena such as giant SHE [3–5], inverse SHE [6–10], and quantum SHE [11–13], have also been widely studied. SHE provides a powerful tool for controlling spins electrically, thus has significant applications for realizing low-power spintronic devices [2].

The origin of SHE can be attributed to either extrinsic impurity scattering [14] or intrinsic spin-orbit coupling (SOC) [15,16]. In intrinsic SHE, the SOC serves as an effective magnetic field that is opposite for spin up and down, leading to a net spin Hall current. For instance, in 2D electronic gases, the Rashba SOC yields a spin Hall conductivity $e/8\pi$, which is a universal constant that does not depend on the underlying material properties [16]. Here the spin current operator is generally defined by $\mathbf{J}_s = \frac{1}{2}\{\frac{\hbar}{2}\sigma_z, \mathbf{v}\}_+$, where the Pauli matrix σ_z is the z component of the rank-1 spin vector, $\{\cdot, \cdot\}_+$ denotes

the anticommutator, and \mathbf{v} is the velocity operator. In this sense, the charge current operator $\mathbf{J}_c = q\sigma_0\mathbf{v}$ can be viewed as rank-0, where σ_0 is the 2×2 identity matrix and q is the carrier charge. For electrons with half spin, the spin transport has hitherto been restricted to the rank-1 spin vector.

Recent theoretical and experimental advances in the study of unconventional spin-1 fermionic excitations have opened a new perspective towards the realization of novel quantum phases and dynamics in large-spin systems, where higher-rank spin tensors exist and play a crucial role [17]. For example, there are five linearly independent rank-2 spin quadrupole tensors that characterize the spin nematics in a spin-1 system [18]. It has been recognized that fermions (e.g., electrons and ultracold fermionic atoms) in crystals and optical lattices are constrained by space group symmetries rather than the Poincaré symmetry. Therefore exotic quasiparticles, like spin-1 fermionic excitations associated with triply degenerate band touching points, can emerge without counterparts in the quantum field theory [19–22] and certain experimental signatures have been observed recently [23]. Moreover, large (pseudo)spins (≥ 1) are easily accessible in experiments for ultracold atoms, superconducting qubits, and trapped ions with multiple (pseudo)spin states [24–27], which can host interesting quantum phases [28–33] and topological states [34–38].

While these works reveal many fascinating phenomena, spin transport in large spin systems, particularly when involving higher-rank spin tensors, remains largely unexplored yet. A natural question is whether there is an intrinsic higher-rank spin tensor Hall effect (STHE) in which a net spin tensor

^{*}These authors contributed equally to this work.

[†]chuanwei.zhang@utdallas.edu

current can be driven by an external field in the longitudinal direction, while both lower-rank spin and charge currents vanish. If it does exist, what is the physical picture of spin tensor current and can the spin tensor Hall conductivity be a universal constant independent of detailed material properties? Can we realize and observe the STHE in a realistic physical system?

In this work, we address these important questions by defining and characterizing the *universal STHE*, and exploring its symmetry protection and experimental realization with ultracold gases. Our main results are the following.

(i) We define spin tensor currents of different ranks in a large-spin system and introduce the concept of STHE. We develop a minimal spin-1 model with intrinsic SOC for realizing the rank-2 STHE. We find that the rank-2 spin tensor Hall conductivity is a universal constant $q/8\pi$, which is independent of detailed model parameters, while both rank-0 charge and rank-1 spin Hall conductivities are zero. Such rank-2 STHE requires the violation of time-reversal symmetry (TRS) but can be protected by a unique pseudo-TRS associated with the rank-2 spin tensor.

(ii) We propose an experimental scheme for realizing and detecting the rank-2 STHE. This is done by utilizing pseudospin-1 ultracold fermionic atoms in a 2D optical lattice, which is built upon recent experimental advances on realizations of 2D SOC for pseudospin-1/2 atoms [39]. We further show that the rank-2 STHE can be observed by measuring the spin tensor accumulation.

(iii) We provide a general route towards the generalization of the higher-rank STHE for larger spins, using the SU(2) subalgebra and generalized Gell-Mann matrix representation of the SU(N) group. For instance, we showcase a generalization of the rank-2 STHE in a spin-3/2 model.

II. SPIN TENSOR CURRENT AND HALL EFFECT

In a spin-1/2 system, the rank-1 spin vectors are defined by Pauli matrices $\sigma_{x,y,z}$, which are the generators of SU(2) group, and there is no rank-2 spin tensor as $\{\sigma_i, \sigma_j\}_+ = 2\delta_{ij}$ (where $i, j = x, y, z$). However, the full characterization of a spin-1 system requires the generators of SU(3) group that include three rank-1 spin vectors and five rank-2 spin tensors. In this case, the spin vectors $F_{x,y,z}$ are the generators of SO(3) group in the spin-1 representation and the spin tensors are defined by the anticommutator [17]

$$N_{ij} = \frac{1}{2}\{F_i, F_j\}_+ - \delta_{ij}\frac{\mathbf{F}^2}{3}, \quad (1)$$

where only five of the nine spin tensors are linearly independent because $N_{ij} = N_{ji}$ and $\sum_i N_{ii} = 0$ [40]. Therefore, to adequately describe the spin transport in a spin-1 system, it is inevitable to involve both spin vectors and tensors, while the latter remains unexplored yet. According to the conventional spin current operator \mathbf{J}_s , the rank-1 spin and rank-2 spin tensor current operators for a spin-1 system can be defined as

$$\mathbf{J}_1^z = \frac{1}{2}\{\hbar F_z, \mathbf{v}\}_+, \quad \mathbf{J}_2^{zz} = \frac{1}{2}\{\hbar N_{zz}, \mathbf{v}\}_+, \quad (2)$$

where $F_z = \text{diag}(1, 0, -1)$ and $N_{zz} = F_z^2 - \frac{2}{3}F_0 = \text{diag}(\frac{1}{3}, -\frac{2}{3}, \frac{1}{3})$. Here F_0 is the 3×3 identity matrix and the rank-0 charge current operator becomes $\mathbf{J}_0 = qF_0\mathbf{v}$. Because

$F_z|m_z\rangle = m_z|m_z\rangle$ with the spin quantum number $m_z = 0$ and ± 1 , \mathbf{J}_1^z measures the conventional spin current, i.e., the counterflow of spin up and down components. The spin component $|0\rangle$ has no contribution to the rank-1 spin current. On the other hand, the rank-2 spin tensor current operator can be decomposed into two parts as $\mathbf{J}_2^{zz} = \frac{1}{2}\{\hbar F_z^2, \mathbf{v}\}_+ - \frac{2\hbar}{3q}\mathbf{J}_0$. Because $|\pm 1\rangle$ are degenerate for F_z^2 as $F_z^2|m_z\rangle = m_z^2|m_z\rangle$, the first term measures the cocurrent of spin up and down components when they move in the same direction. Thus it vanishes for a pure rank-1 spin current in the presence of TRS. The second term is proportional to \mathbf{J}_0 . Note that for a pure rank-0 charge current (without any spin polarization), the contributions from the two terms cancel out each other since $\text{Tr}(N_{zz}) = 0$, leading to $\langle \mathbf{J}_2^{zz} \rangle = 0$. Therefore \mathbf{J}_2^{zz} measures a unique rank-2 spin tensor current in which both spin up and down particles propagate in the same direction, opposite to that of spin $|0\rangle$.

According to the widely studied intrinsic rank-1 SHE in the 2D Rashba electron gas [16], a transverse rank-1 spin current can be driven by an external field in the longitudinal direction, as shown in Fig. 1(a). The Rashba SOC obeys the TRS that guarantees no transverse charge current. In the same manner, we define the rank-2 STHE as a transverse rank-2 spin tensor current driven by a field in the longitudinal direction while no transverse lower-rank spin or charge current, as shown in Fig. 1(b), which requires the violation of TRS. In the following, we will construct a minimal spin-1 model to demonstrate that the rank-2 STHE can arise from an intrinsic spin-tensor-momentum coupling (STMC) and be guaranteed by a unique pseudo-TRS associated with the rank-2 spin tensor.

III. MODEL HAMILTONIAN

A general form of SOC in a spin-1 system involves both spin vectors and tensors [22]. In order to find a suitable SOC for the rank-2 STHE, we adopt the Gell-Mann matrix representation $\{\lambda_n\}$ (where $n = 1, \dots, 8$) of the SU(3) group, which can be further grouped into three subsets

$$\boldsymbol{\tau}_T = \{\lambda_1, \lambda_2, \lambda_3\}, \quad \boldsymbol{\tau}_U = \{\lambda_4, \lambda_5, \lambda_+\}, \quad \boldsymbol{\tau}_V = \{\lambda_6, \lambda_7, \lambda_-\}, \quad (3)$$

that generate three different SU(2) subalgebras in the spin subspaces spanned respectively by $\{|1\rangle, |0\rangle\}_T$, $\{|1\rangle, |-1\rangle\}_U$, and $\{|0\rangle, |-1\rangle\}_V$, where $\lambda_{\pm} = \frac{\sqrt{3}}{2}\lambda_8 \pm \frac{1}{2}\lambda_3$ [42]. It is easy to show that each subset satisfies the commutation relation $[\tau_{\Gamma,i}, \tau_{\Gamma,j}] = 2i\varepsilon_{ijk}\tau_{\Gamma,k}$ since $P_{\Gamma}\tau_{\Gamma,i}P_{\Gamma} = \sigma_i$, where ε_{ijk} is the Levi-Civita symbol and P_{Γ} is the projection operator onto the spin subspace Γ , e.g., $P_T = |1\rangle\langle 1| + |0\rangle\langle 0|$ for $\Gamma = T$ [40]. Therefore $\boldsymbol{\tau}_{\Gamma}$ spans the symmetry group of an effective quantum spin 1/2 in the spin subspace Γ . In this representation, the spin vectors F_i can be expanded as $F_x = (\lambda_1 + \lambda_6)/\sqrt{2}$, $F_y = (\lambda_2 + \lambda_7)/\sqrt{2}$, and $F_z = (\lambda_3 + \sqrt{3}\lambda_8)/2$.

The advantage of introducing the SU(2) subalgebras is that it allows to expand a general spin-1 SOC as the superposition of a set of effective spin-1/2 SOC's in different spin subspaces. For instance, we consider the Rashba SOC in the spin subspace Γ as

$$H_{\Gamma} = \frac{\mathbf{p}^2}{2m^*} - \frac{\lambda}{\hbar}\boldsymbol{\tau}_{\Gamma} \cdot (\hat{\mathbf{z}} \times \mathbf{p}), \quad (4)$$

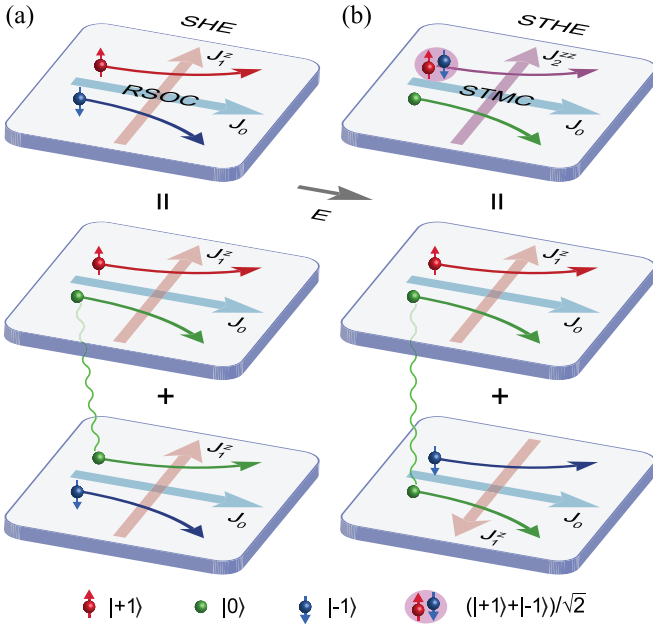


FIG. 1. (a) The intrinsic rank-1 SHE arises from the Rashba spin-orbit coupling (RSOC) in a (pseudo)spin-1 system (top). The external field \mathbf{E} drives a charge current \mathbf{J}_0 in the longitudinal direction and a transverse spin current \mathbf{J}_1^z from the deflection of spin up and down components to opposite transverse directions. The spin-1 RSOC can be decomposed into the superposition of two effective spin-1/2 RSOCs which respectively lead to the SHEs in the spin subspaces $\{|+1\rangle, |0\rangle\}$ (middle) and $\{|0\rangle, |-1\rangle\}$ (bottom). The two decomposed SHEs have same spin current and are coupled via the shared $|0\rangle$ that is linked by the green wavy line between the middle and lower panels. (b) The intrinsic rank-2 STHE arising from the STMC in a (pseudo)spin-1 system (top). Here the transverse rank-2 spin tensor current \mathbf{J}_2^{zz} comes from the deflection of spin components $|0\rangle$ and $(|+1\rangle + |-1\rangle)/\sqrt{2}$ to opposite transverse directions. The STMC can be decomposed into the superposition of two conjugate effective spin-1/2 RSOCs which lead to two opposite SHEs in the spin subspaces $\{|+1\rangle, |0\rangle\}$ (middle) and $\{|0\rangle, |-1\rangle\}$ (bottom), respectively. The coupling between the two decomposed SHEs with opposite spin currents via the shared $|0\rangle$ is indicated by the green wavy line.

where m^* is the effective mass and λ is the SOC constant. Then the spin-1 Rashba SOC can be expanded as the superposition of H_T and H_V because $\mathbf{F} \cdot (\hat{\mathbf{z}} \times \mathbf{p}) = \frac{1}{\sqrt{2}}(\boldsymbol{\tau}_T + \boldsymbol{\tau}_V) \cdot (\hat{\mathbf{z}} \times \mathbf{p})$. Furthermore, both H_T and H_V lead to a rank-1 SHE in their own spin subspaces, however, they are not independent by sharing the common basis $|0\rangle$. Therefore the intrinsic rank-1 SHE due to the Rashba SOC in a spin-1 system can be understood as two hybridized rank-1 SHEs with same spin currents in the spin subspaces $\{|1\rangle, |0\rangle\}_T$ and $\{|0\rangle, |-1\rangle\}_V$, respectively, as depicted in Fig. 1(a). Using this hierarchy expansion, we can construct the desired large-spin SOC for the higher-rank STHE from the elementary spin-1/2 SOC.

To realize the rank-2 STHE, both spin up and down particles are required to propagate in the same direction, opposite to that of spin $|0\rangle$. This can be achieved by the superposition of H_T and H_V^* where $H_V^* = e^{-iF_x\pi} H_T e^{iF_x\pi}$ yields an opposite spin current to that of H_T under the spin flip operation, as

depicted in Fig. 1(b). Then the rank-2 STHE can be realized by the spin-1 model Hamiltonian

$$H_{F=1} = \frac{\mathbf{p}^2}{2m^*} - \frac{1}{\sqrt{2}} \frac{\lambda}{\hbar} (\boldsymbol{\tau}_T + \boldsymbol{\tau}_V^*) \cdot (\hat{\mathbf{z}} \times \mathbf{p}), \quad (5)$$

where $\frac{1}{\sqrt{2}}(\boldsymbol{\tau}_T + \boldsymbol{\tau}_V^*) \cdot (\hat{\mathbf{z}} \times \mathbf{p}) = -p_y F_x + 2p_x N_{yz}$ depicts the STMC with the spin tensor $N_{yz} = \{F_y, F_z\}_+/2 = (\lambda_2 - \lambda_7)/2\sqrt{2}$. The resulting band structure is plotted in Fig. 2(a), which exhibits a triply degenerate point at $\mathbf{p} = 0$ and $E = 0$. When the Fermi energy E_F lays above the triply degenerate point, the Fermi surfaces are three concentric circles.

IV. UNIVERSAL RANK-2 SPIN TENSOR HALL CONDUCTIVITY

The rank-2 spin tensor Hall conductivity can be calculated from the Kubo formula

$$\sigma_{xy}^{zz} = q\hbar \int \frac{d^2\mathbf{k}}{(2\pi)^2} \sum_{n \neq n'} (f_{n'\mathbf{k}} - f_{n\mathbf{k}}) \times \frac{\text{Im}[\langle n'\mathbf{k} | J_{2,x}^{zz} | n\mathbf{k} \rangle \langle n\mathbf{k} | v_y | n'\mathbf{k} \rangle]}{(E_{n\mathbf{k}} - E_{n'\mathbf{k}})^2}, \quad (6)$$

where n (n') is the band index, and $f_{n\mathbf{k}} = [e^{(E_{n\mathbf{k}} - E_F)/k_B T} + 1]^{-1}$ is the Fermi function. Applying the Kubo formula to the model Hamiltonian (5) with $H_{F=1} |n\mathbf{k}\rangle = E_{n\mathbf{k}} |n\mathbf{k}\rangle$ and $\mathbf{v} = \partial_{\mathbf{p}} H_{F=1}$, we find a nonzero rank-2 spin tensor Hall conductivity

$$\sigma_{xy}^{zz} = \frac{q}{8\pi}, \quad (7)$$

when the Fermi energy is above the triply degenerate point for $E_F > 0$, as shown in Fig. 2(b). Furthermore, the quantized rank-2 spin tensor Hall conductivity is a universal constant, i.e., it is independent of the detailed model parameters such as the effective mass m^* or STMC constant λ (see Ref. [40] for analytical proof). Below the triply degenerate point for $E_F < 0$, the rank-2 spin tensor Hall conductivity σ_{xy}^{zz} jumps from 0 to $q/8\pi$ as the Fermi energy increases from the band bottom to the triply degenerate point. We also calculate the rank-1 spin Hall conductivity σ_{xy}^z and rank-0 charge Hall conductivity σ_{xy} , as shown in Fig. 2(b), that are obtained from the Kubo formula by substituting the corresponding spin and charge current operators into Eq. (6). Apparently, they both vanish for arbitrary Fermi energy. To compare with, we remark that the rank-1 SHE due to the spin-1 Rashba SOC $\mathbf{F} \cdot (\hat{\mathbf{z}} \times \mathbf{p})$ yields a universal rank-1 spin Hall conductivity $\sigma_{xy}^z = q/2\pi$, while $\sigma_{xy}^{zz} = \sigma_{xy} = 0$. Therefore the model Hamiltonian Eq. (5) describes a simple yet nontrivial system exhibiting the universal STHE.

V. PSEUDO-TRS AND PSEUDOSPIN DYNAMICS

To understand the physical nature of the rank-2 STHE, we remark that the STMC breaks the TRS since the spin tensors are even under time-reversal operation as $\mathcal{T} N_{ij} \mathcal{T}^{-1} = N_{ij}$, while both spin vectors F_i and momentum \mathbf{p} are odd. Here

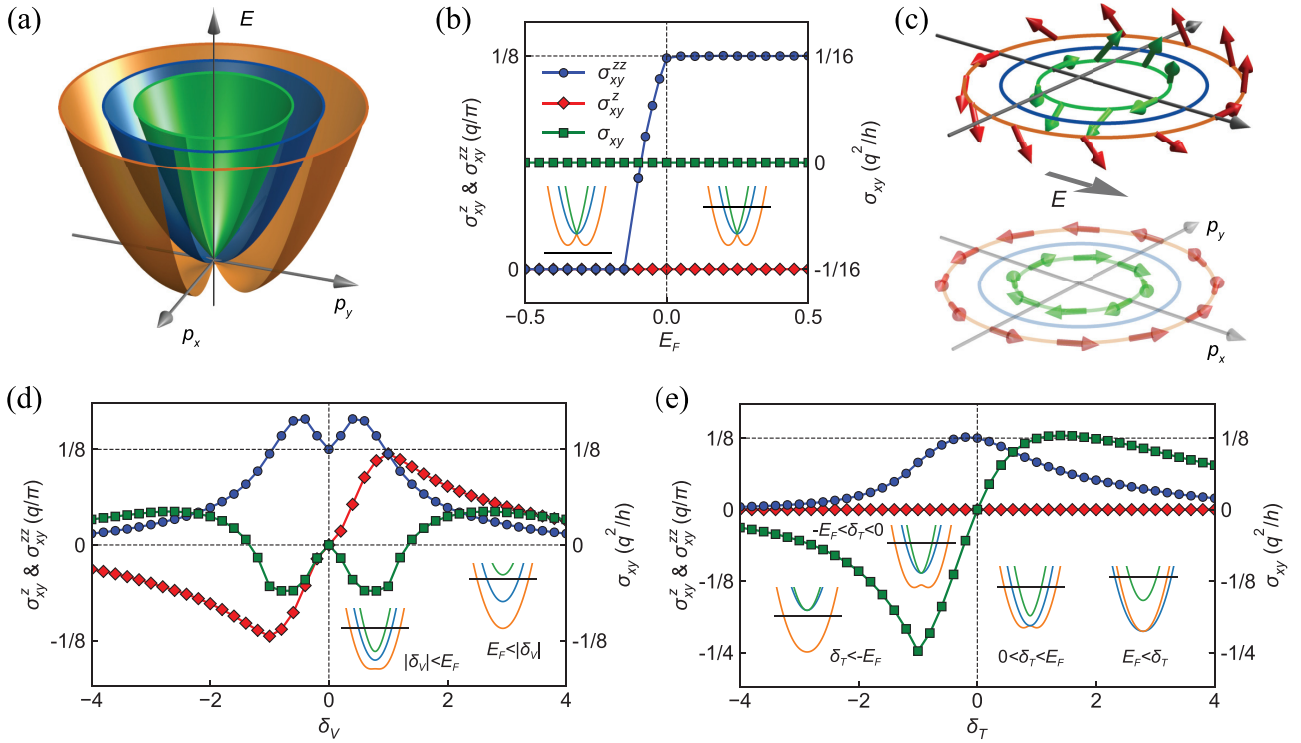


FIG. 2. (a) Schematic band structure of the model Hamiltonian with STMC. There is a triply degenerate point above which the Fermi surfaces are three concentric circles. (b) The rank-2 spin tensor Hall conductivity σ_{xy}^{zz} , rank-1 spin Hall conductivity σ_{xy}^z , and rank-0 charge Hall conductivity σ_{xy} as a function of the Fermi energy E_F . When the Fermi energy shifts above the triply degenerate point, σ_{xy}^{zz} jumps to the quantized value of $q/8\pi$, while both σ_{xy}^z and σ_{xy} remain zero. (c) The pseudospin texture on the concentric Fermi surfaces in the presence (absence) of an external field \mathbf{E} in the upper (lower) panel. The pseudospin is defined as $|\uparrow\rangle = (|1\rangle + |-1\rangle)/\sqrt{2}$ and $|\downarrow\rangle = |0\rangle$. The external field displaces the Fermi surfaces along the field direction and tilts the pseudospins with opposite transverse momenta to opposite out-of-plane directions (top). [(d) and (e)] The three Hall conductivities in (b) are displayed as a function of the spin-vector Zeeman field δ_V in (d) and spin-tensor Zeeman field δ_T in (e) for a Fermi energy above the triply degenerate point. The Fermi energy $E_F = 1$ and momentum $p_F = 1$ are taken as units for energy and momentum. The corresponding dimensionless parameters are set as $m^* = 0.5$ and $\lambda = 0.7$. The insets of (b), (d), and (e) exhibit the typical band structures and Fermi levels in different parameter regions.

$\mathcal{T} = e^{-iF_y\pi} \mathcal{K}$ is the TRS operator for spin 1 and \mathcal{K} is the complex conjugate operator. Furthermore, the STMC in Eq. (5) can be understood as coupled Rashba SOC and its conjugate in different spin subspaces $\{|1\rangle, |0\rangle\}_T$ and $\{|0\rangle, |-1\rangle\}_V$ through the shared $|0\rangle$. It yields a coherent current of spin $\frac{1}{\sqrt{2}}(|1\rangle + |-1\rangle)$ flowing in opposite direction to that of spin $|0\rangle$, as shown in Fig. 1(b). It is noted that the Hamiltonian Eq. (5) preserves a unique pseudo-TRS

$$\Xi H_{F=1}(\mathbf{p}) \Xi^{-1} = H_{F=1}(-\mathbf{p}), \quad (8)$$

where $\Xi = e^{-iN_y\pi} \mathcal{K}$ is the pseudo-time-reversal operator. The pseudo-TRS ensures that if there is a current of $\frac{1}{\sqrt{2}}(|1\rangle + |-1\rangle)$, there must be an opposite current of $|0\rangle$ since the doublet is interchanged as $\Xi \frac{1}{\sqrt{2}}(|1\rangle + |-1\rangle) = |0\rangle$ and $\Xi |0\rangle = -\frac{1}{\sqrt{2}}(|1\rangle + |-1\rangle)$. Therefore the rank-2 STHE can be protected by the unique pseudo-TRS associated with the rank-2 spin tensor, which does not exist in spin-1/2 systems.

A more intuitive picture can be given by the pseudospin dynamics analysis in which the pseudospins are defined as $|\uparrow\rangle = \frac{1}{\sqrt{2}}(|1\rangle + |-1\rangle)$ and $|\downarrow\rangle = |0\rangle$ that are orthogonal to $|\ominus\rangle = \frac{1}{\sqrt{2}}(|1\rangle - |-1\rangle)$. Then the rank-2 spin tensor current is equivalent to the rank-1 pseudospin current in the new basis.

When projecting onto the pseudospin subspace $\{|\uparrow\rangle, |\downarrow\rangle\}$, $H_{F=1}$ yields a Rashba pseudospin-orbit coupling that exerts an effective momentum-dependent Zeeman field $\mathbf{\Delta} = \frac{2\lambda}{\hbar} \hat{z} \times \mathbf{p}$ on the pseudospins (see Ref. [40] for details). Thus the pseudospins aligned with $\mathbf{\Delta}$ lead to the helical pseudospin texture on the Fermi surfaces, as shown in the lower panel of Fig. 2(c). Here the middle Fermi surface (with blue color) is from the $|\ominus\rangle$ that has no pseudospin. Under an electric field \mathbf{E} , the particles are accelerated as $\dot{\mathbf{p}} = q\mathbf{E}$ that displaces the Fermi surfaces and varies the Zeeman field as $\mathbf{\Delta}(t) = \frac{2q\lambda}{\hbar} \hat{z} \times \mathbf{E}$. Then the pseudospins with opposite transverse momenta on the displaced Fermi surfaces are tilted to opposite out-of-plane directions by $\mathbf{\Delta}(t)$ as

$$n_{s,z} = \frac{q\hbar^2 E_x p_y}{2\lambda p^3}, \quad (9)$$

where $n_{s,z}$ is the z component of the pseudospin vector \mathbf{n}_s and $\mathbf{E} = E_x \hat{x}$ is in the x direction (see Ref. [40] for derivations), as depicted in the upper panel of Fig. 2(c). It gives rise to a rank-1 pseudospin current arising from the deflection of pseudospin components $|\uparrow\rangle$ and $|\downarrow\rangle$ to opposite transverse directions, i.e., the rank-2 spin tensor current in the bare spin basis [see Fig. 1(b)].

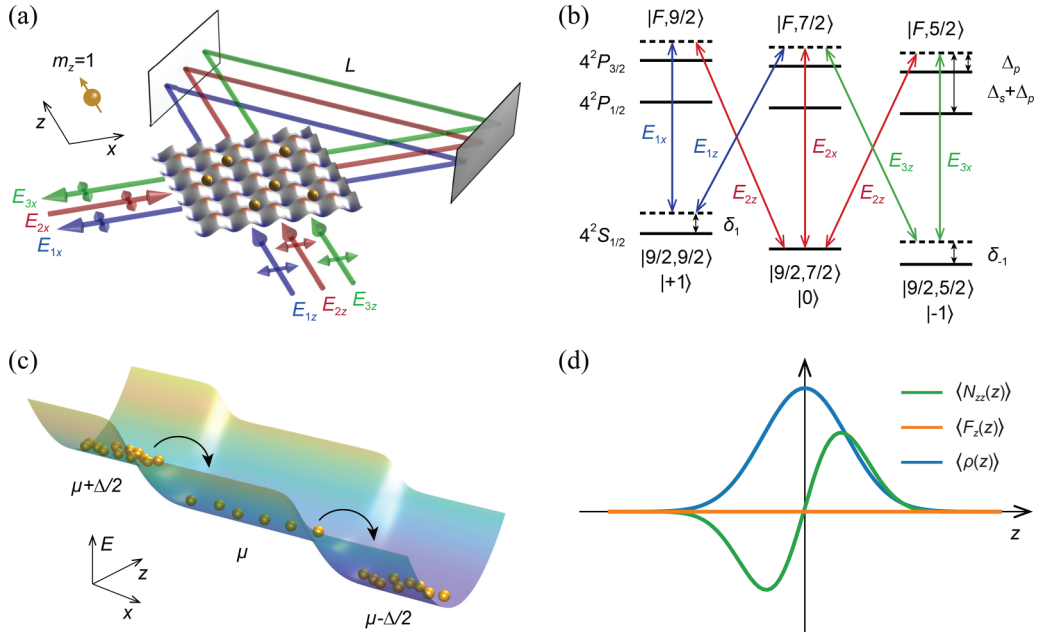


FIG. 3. (a) Sketch of the experimental setup. Three laser beams $E_{1z,2z,3z}$ are incident in the z direction and one laser beam E_{2x} is incident in the x direction. The laser beams are reflected by two mirrors in the triangular optical path L and form an optical lattice in the intersecting region. The double-headed arrows indicate the polarization of the laser beams. In this setup, the spin quantization axis is along the z direction. (b) Energy level diagram of the ^{40}K atom, showing how the STMC can be realized through the Raman couplings induced by the laser beams in (a). Here $|F, m_F\rangle$ denotes the hyperfine states of ^{40}K atom and the pseudospin-1 states are defined as $|+1\rangle = |9/2, 9/2\rangle$, $|0\rangle = |9/2, 7/2\rangle$, and $|-1\rangle = |9/2, 5/2\rangle$. Δ_s is the fine-structure splitting and $\delta_{1(-1)}$ is the two-photon detuning. (c) Energy profile of the transverse harmonic trap and the longitudinal bias potential. The cold atoms are transported from the left to the right reservoirs through the middle conducting channels. (d) Schematic local spin tensor density $\langle N_{zz}(z) \rangle$, local spin density $\langle F_z(z) \rangle$, and local density of states $\langle \rho(z) \rangle$ in the middle conducting region of (c). The antisymmetric $N_{zz}(z)$ indicates the accumulation of spin components $|0\rangle$ and $(|1\rangle + |-1\rangle)/\sqrt{2}$ at opposite lateral edges of the system due to the rank-2 SHE, while the vanishing $\langle F_z(z) \rangle$ and symmetric $\langle \rho(z) \rangle$ manifest no rank-1 spin or rank-0 particle accumulation in the presence of pseudo-TRS.

VI. EFFECT OF ZEEMAN FIELDS

Generally, for a spin-1 system discussed above, the Zeeman fields contain both spin-vector and spin-tensor terms as $-\delta_V F_z - \delta_T F_z^2$. Both fields lift the triply degenerate point at $\mathbf{p} = 0$ and break the pseudo-TRS that spoils the universality of the rank-2 spin tensor Hall conductivity. For a given Fermi energy $E_F > 0$ above the triply degenerate point, we show the charge, spin, and spin tensor Hall conductivities of different ranks as a function of δ_V and δ_T in Figs. 2(d) and 2(e), respectively.

For the spin-vector Zeeman field $-\delta_V F_z$, changing the sign of δ_V is equivalent to a \mathbb{Z}_2 rotation between spin components $|1\rangle$ and $|-1\rangle$, under which the spin-tensor polarization $\langle N_{zz} \rangle$ is unchanged while the spin-vector polarization $\langle F_z \rangle$ gains a minus sign, indicating symmetric and antisymmetric responses from σ_{xy}^{zz} and σ_{xy}^z , as shown in Fig. 2(d). Moreover, due to the breaking of both TRS and pseudo-TRS, a nonzero charge Hall conductivity σ_{xy} emerges and is symmetric with respect to δ_V . As $|\delta_V|$ ramps up, the magnitudes of all three Hall conductivities firstly increase to their maxima and then decrease. In particular, σ_{xy} reverses sign at a critical value. It is noted that the top band shifts above the Fermi energy for $|\delta_V| > E_F$ and $|\sigma_{xy}^z|$ reaches its maximum value around $\delta_V = \pm E_F$ [see Fig. 2(d) and its insets]. When $\delta_V \rightarrow \pm\infty$, all three Hall conductivities approach 0 since the system becomes a flat-band insulator.

On the other hand, the spin-tensor Zeeman field $-\delta_T F_z^2$ has the same effect on $|\pm 1\rangle$ since they are degenerate for F_z^2 . Therefore σ_{xy}^{zz} is asymmetric while σ_{xy}^z remains zero, as shown in Fig. 2(e). σ_{xy} is also asymmetric and reverses sign at $\delta_T = 0$. In this case, the triply degenerate point splits into a doubly degenerate point and a nondegenerate point at $\mathbf{p} = 0$. When $\delta_V < 0$, it shifts the doubly degenerate point upward and the top two bands are above the Fermi energy for $\delta_T < -E_F$ [see the insets of Fig. 2(e)]. When $\delta_V > 0$, the doubly degenerate point is pushed down and all three bands remain intersecting the Fermi level. Therefore σ_{xy}^{zz} decreases faster in the negative side. It is also noticed that σ_{xy} shows a dip around $\delta_T = -E_F$.

VII. EXPERIMENTAL SCHEME FOR THE RANK-2 STHE

Here we propose an experimental scheme to realize and detect the rank-2 STHE with ultracold gases. As illustrated in Fig. 3(a), the fermionic cold atoms are loaded into an optical lattice created by two laser beams E_{2x} and E_{2z} that are incident in x and z directions and reflected by two mirrors. The superposition of incident and reflected beams generate two standing waves $\mathbf{E}_{2x} = \hat{z}E_{2x}e^{i(\phi_{2x} + \phi_{2z} + \phi_L)/2} \cos(k_0x + \alpha)$ and $\mathbf{E}_{2z} = \hat{x}E_{2z}e^{i(\phi_{2z} + \phi_{2x} + \phi_L)/2} \cos(k_0z + \beta)$ that give rise to the optical lattice potential $V_0(\mathbf{r}) = V_{0x} \cos^2(k_0x + \alpha) + V_{0z} \cos^2(k_0z + \beta)$, where $\alpha(\beta) = [\phi_{2x(z)} - \phi_{2z(x)} - \phi_L]/2$. Here $\phi_{2x(z)}$ are the initial phases of $E_{2x(z)}$ and $\phi_L = k_0L$ is the phase

accumulated by the beams when traveling through the triangular optical path L (see Fig. 3(a)). To realize the desired STMC in Eq. (5), another two laser beams E_{1z} and E_{3z} are incident in the z direction that generates four plane waves $\mathbf{E}_{1z} = \hat{x}\bar{E}_{1z}e^{i(k_0z+\phi_1)}$, $\mathbf{E}_{3z} = \hat{x}\bar{E}_{3z}e^{i(k_0z+\phi_3)}$, $\mathbf{E}_{1x} = \hat{z}\bar{E}_{1x}e^{i(-k_0x+\phi_1+\phi_L-\delta\phi_{1L})}$, and $\mathbf{E}_{3x} = \hat{z}\bar{E}_{3x}e^{i(-k_0x+\phi_3+\phi_L-\delta\phi_{3L})}$ at the intersecting region where the latter two are the reflected beams [see Fig. 3(a)]. Here $\phi_{1(3)}$ are the initial phases of $E_{1(3)z}$ and $\delta\phi_{1(3)L} = (\omega_2 - \omega_{1(3)})L/c$.

To realize the spin-1 model, we consider three hyperfine states of ^{40}K atoms that define a pseudospin 1 as $|1\rangle = |9/2, 9/2\rangle$, $|0\rangle = |9/2, 7/2\rangle$, and $|-1\rangle = |9/2, 5/2\rangle$ [see Fig. 3(b)]. The Raman coupling induced by the laser beams can hybridize the three hyperfine states while the coupling to other hyperfine states $|9/2, m_F < 5/2\rangle$ can be suppressed by a sufficiently large detuning. In the basis of $\{|1\rangle, |0\rangle, |-1\rangle\}$, the Raman potential reads

$$\begin{pmatrix} 0 & M_x - M_y e^{i\delta\phi_{1L}} & 0 \\ M_x - M_y e^{-i\delta\phi_{1L}} & 0 & M'_x - M'_y e^{-i\delta\phi_{3L}} \\ 0 & M'_x - M'_y e^{i\delta\phi_{3L}} & 0 \end{pmatrix}, \quad (10)$$

where $M_x^{(l)} = M_{0x}^{(l)} \cos(k_0x + \alpha) \sin(k_0z + \beta)$ and $M_y^{(l)} = M_{0y}^{(l)} \cos(k_0z + \beta) \sin(k_0x + \alpha)$. The desired STMC in Eq. (5) requires the Raman potential to take the form of $M_x(\lambda_1 + \lambda_6) + M_y(\lambda_2 - \lambda_7)$ that demands $M_{0x(y)} = M'_{0x(y)}$ and $\delta\phi_{1L} = \delta\phi_{3L} = \pi/2$ (see Ref. [40] and references [39,41,44] therein for details). This can be achieved by adjusting the laser frequencies ω_n and amplitudes $\bar{E}_{nx(y)}$. Meanwhile, the Zeeman terms $-\delta_V F_z - \delta_T F_z^2$ can be induced by the two-photon detunings with $\delta_1 = \delta_T + \delta_V$ and $\delta_{-1} = \delta_T - \delta_V$, as shown in Fig. 3(b). A similar setup with two standing waves and two plane waves has been used to realize the 2D SOC for pseudospin-1/2 cold atoms [39,44,45].

To trigger and detect the rank-2 STHE, we further consider a bias potential $\mu \pm \Delta/2$ along the x direction and a transverse harmonic potential $\frac{1}{2}m^*\omega^2z^2$ that traps atoms in the z direction [see Fig. 3(c)]. Note that the oscillator length $l_\omega = \sqrt{\hbar/m^*\omega}$ is much larger than the laser wavelength $2\pi/k_0$, while the trap potential is much weaker and smoother in the x direction and can be treated as a constant. The bias potential for driving atoms to move from the left to the right reservoirs can be achieved by shaping the external potential, that has been used to realize the quantum transport in ultracold gases [46,47]. Overall, we consider a quasi-1D system in the middle conducting region of Fig. 3(c) that can be described by the low-energy effective Hamiltonian $H = \mathbf{p}^2/2m^* + \frac{\lambda}{\hbar}(p_z F_x + 2p_x N_{yz}) - \delta_V F_z - \delta_T F_z^2 + \frac{1}{2}m^*\omega^2z^2$, where λ is determined by the Rabi frequencies in the two-photon transitions [40]. Then the transverse rank-2 spin tensor current generated by the counterflow of spin components $|0\rangle$ and $\frac{1}{\sqrt{2}}(|1\rangle + |-1\rangle)$ leads to the accumulation of cold atoms in the two different states at opposite lateral edges [see Fig. 1(b)]. This results in an antisymmetric local spin tensor density $\langle N_{zz}(z) \rangle$ in the transverse direction, while the pseudo-TRS guarantees no lower-rank spin or particle accumulation that features a vanishing local spin density $\langle F_z(z) \rangle$ and symmetric local

density of states $\langle \rho(z) \rangle$ for $\delta_{V(T)} = 0$, as illustrated in Fig. 3(d). Therefore the unique spin tensor accumulation can be detected as the signature of the rank-2 STHE, similar as the spin accumulation for the rank-1 SHE in the 2D electron gas [14].

To explicitly show the rank-2 spin tensor accumulation, we calculate the local spin tensor density

$$\langle N_{zz}(\mathbf{r}) \rangle = \int_{\mu - \frac{\Delta}{2}}^{\mu + \frac{\Delta}{2}} \frac{dE}{\pi} \sum_{n, k_x} \text{Im} \left[\frac{\Theta(v_x) \psi_{n, k_x}^\dagger(\mathbf{r}) N_{zz} \psi_{n, k_x}(\mathbf{r})}{E - E_{n, k_x} - i0^+} \right], \quad (11)$$

where $H \psi_{n, k_x}(\mathbf{r}) = E_{n, k_x} \psi_{n, k_x}(\mathbf{r})$ and $\Theta(v_x)$ is the Heaviside step function of the group velocity $v_x = \partial E_{n, k_x} / \hbar \partial k_x$ that counts the conducting channels to the positive x direction within the biased potential energies. Because the wave function $\psi_{n, k_x}(\mathbf{r})$ is a plane wave in the x direction, the local spin tensor density depends only on z as $\langle N_{zz}(\mathbf{r}) \rangle = \langle N_{zz}(z) \rangle$. Meanwhile, the local spin density $\langle F_z(z) \rangle$ and local density of states $\langle \rho(z) \rangle$ can also be calculated from Eq. (11) by replacing N_{zz} with F_z and F_0 , respectively. For $\delta_{V(T)} = 0$ and under the transverse harmonic trap, the 2D energy bands [see Fig. 2(a)] are quantized into a set of 1D subbands in Fig. 4(a), which constitute the conducting channels for the rank-2 STHE. Here each group of subbands contains three members whose bottoms are around $(n + \frac{1}{2})\hbar\omega$ (see Ref. [40] for derivations). In Fig. 4(b), we show $\langle N_{zz}(z) \rangle$ as a function of the chemical potential μ for $\Delta \ll \frac{1}{2}\hbar\omega$. Apparently, a rank-2 spin tensor accumulation arises from the antisymmetric distribution of $\langle N_{zz}(z) \rangle$, reflecting the accumulation of spin components $|0\rangle$ and $(|1\rangle + |-1\rangle)/\sqrt{2}$ at opposite lateral edges. However, it is noticed that $\langle N_{zz}(z) \rangle$ is not perfectly antisymmetric around the subband bottoms for $\mu \sim (n + \frac{1}{2})\hbar\omega$ where only two of the three subbands are occupied. This is because the universality of the rank-2 STHE requires the occupation of all three subbands in each group. As μ increases, more subbands are occupied and high harmonics of $\langle N_{zz}(z) \rangle$ emerge [see Fig. 4(b)]. In this case, the local spin density $\langle F_z(z) \rangle$ vanishes everywhere and the local density of states $\langle \rho(z) \rangle$ is perfectly symmetric for arbitrary μ , indicating no lower-rank spin or particle accumulation in the presence of pseudo-TRS.

Now we turn on the Zeeman fields that break the pseudo-TRS and spoil the universality of the rank-2 STHE. As shown in Fig. 4(c), the subbands are split apart from each other around the band bottoms. The rank-2 spin tensor accumulation persists, as shown in Fig. 4(d), and is smeared compared with that in Fig. 4(b). In this case, there are also lower-rank spin and particle accumulations due to the finite lower-rank spin and charge Hall conductivities [see Figs. 3(d) and 3(e)]. These can be revealed by the local spin density $\langle F_z(z) \rangle$ and local density of states $\langle \rho(z) \rangle$, as shown in Figs. 4(e) and 4(g). The asymmetric distribution of $\langle F_z(z) \rangle$ and $\langle \rho(z) \rangle$ reflects the spin and particle accumulation that can be further manifested by extracting their antisymmetric parts $\langle \delta F_z(z) \rangle = \langle F_z(z) \rangle - \langle F_z(-z) \rangle$ and $\langle \delta \rho(z) \rangle = \langle \rho(z) \rangle - \langle \rho(-z) \rangle$, as shown in Figs. 4(g) and 4(h), respectively. The nonzero $\langle \delta F_z(z) \rangle$ and $\langle \delta \rho(z) \rangle$ indicate the accumulation of spin components $|\pm 1\rangle$ and the imbalanced distribution of atoms at opposite lateral edges.

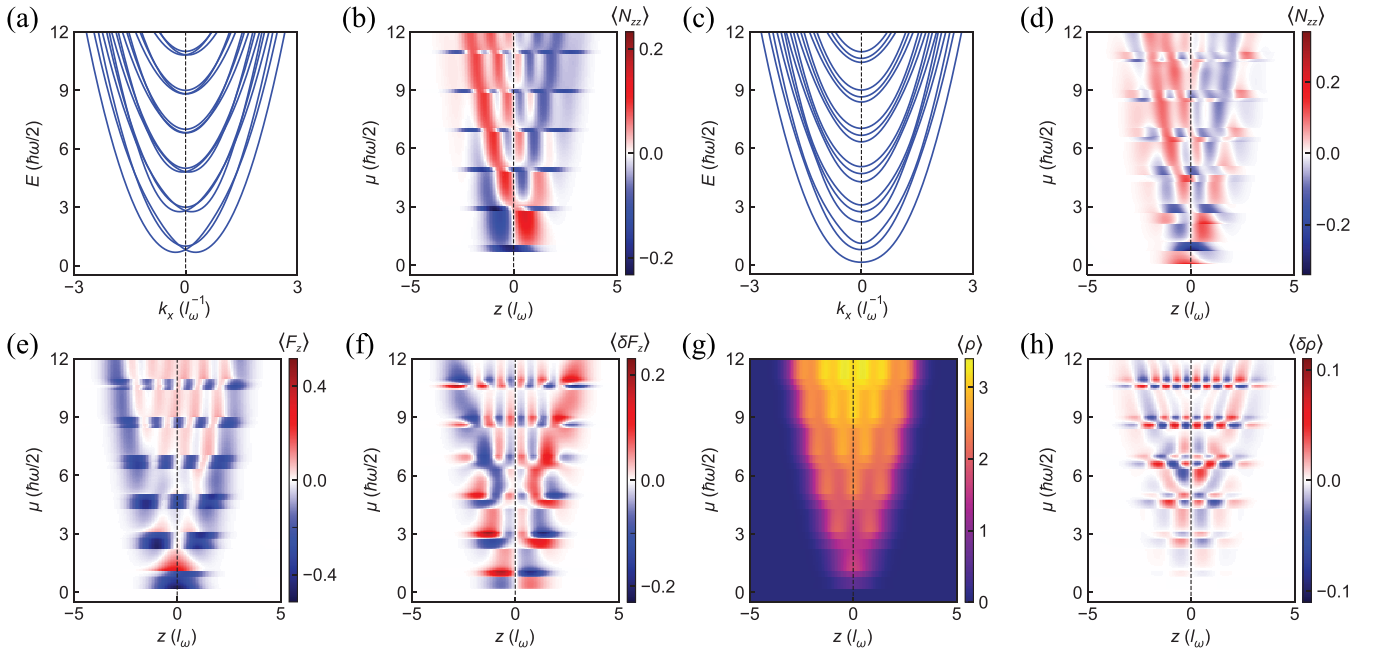


FIG. 4. [(a) and (c)] Energy spectra of quasi-1D ultracold gases with STMC and confined by a transverse harmonic trap. There is no Zeeman field for (a) and finite Zeeman fields $\delta_V = 0.5$ and $\delta_T = 0.3$ for (c). [(b) and (d)] The rank-2 spin tensor accumulation revealed by the local spin tensor density $\langle N_{zz}(z) \rangle$ as a function of the chemical potential μ , corresponding to the energy spectra in (a) and (c), respectively. [(e) and (f)] The rank-1 spin accumulation revealed by the local spin density $\langle F_z(z) \rangle$ and its antisymmetric part $\langle \delta F_z(z) \rangle = \langle F_z(z) \rangle - \langle F_z(-z) \rangle$ that are displayed as a function of μ for the finite Zeeman fields in (c). [(g) and (h)] The rank-0 particle accumulation revealed by the local density of states $\langle \rho(z) \rangle$ and its antisymmetric part $\langle \delta \rho(z) \rangle = \langle \rho(z) \rangle - \langle \rho(-z) \rangle$ for the finite Zeeman fields in (c).

VIII. GENERALIZATION TO LARGER SPINS

Mathematically, it is well-known that a spin- F Hamiltonian can be expanded using the generators of the $SU(N)$ group, where $N = 2F + 1$. These generators are traceless and hermitian, and can be constructed as spin vectors and tensors. The maximum rank of the spin tensor is $N - 1$ that is the rank of the $SU(N)$ group. For instance, there are up to rank-2 spin tensors defined as $N_{ij} = \{F_i, F_j\}_+ / 2 - \delta_{ij} \mathbf{F}^2 / 3$ in a spin-1 system, as discussed above. In principle, higher-rank spin tensors (up to rank- $N - 1$) can be defined in a larger spin system and we can use a Cartan subalgebra $\{F_z, N_{zz}, \dots, N_{zz \dots z}\}$ of $SU(N)$ to define a rank- n spin tensor current operator $\mathbf{J}_n^{zz \dots z} = \frac{1}{2} \{N_{zz \dots z}, \mathbf{v}\}_+$, where $N_{zz \dots z}$ with n subscripts denotes a rank- n spin tensor. Then the rank- n STHE can be naturally introduced for a system with only nonzero rank- n spin tensor current.

To construct a suitable SOC for a rank- n STHE, we firstly need to identify the $SU(2)$ subalgebras of $SU(N)$. This can be achieved by using the generalized Gell-Mann matrices [43]

$$\begin{aligned} \lambda_{j,k}^S &= I_{j,k} + I_{k,j}, \\ \lambda_{j,k}^A &= -i(I_{j,k} - I_{k,j}), \\ \lambda_l^D &= \sqrt{\frac{2}{l(l+1)}} \left(\sum_{m=1}^l I_{m,m} - l I_{l+1,l+1} \right), \end{aligned} \quad (12)$$

where $1 \leq j < k \leq N$, $1 \leq l \leq N - 1$, and $I_{j,k}$ denotes the $N \times N$ matrix whose nonzero elements are 1 in the (j, k) th entry. Then we could write down all different $SU(2)$

subalgebras as

$$\tau_{j,k} = \{ \lambda_{j,k}^S, \lambda_{j,k}^A, c_{j,k}^l \lambda_l^D \}, \quad (13)$$

where the Einstein summation convention is employed for $c_{j,k}^l \lambda_l^D$. Here $c_{j,k}^l$ are some real constants that can be determined by the commutation relation $[\lambda_{j,k}^S, \lambda_{j,k}^A] = 2ic_{j,k}^l \lambda_l^D$ such that the structure constant of the $SU(2)$ subalgebra is maintained. For instance, the rank-2 STHE can also be realized in a spin-3/2 system with the SOC described by $H_{F=\frac{3}{2}} = \mathbf{p}^2 / 2m^* - \frac{\lambda}{\hbar} (\boldsymbol{\tau}_{1,2} + \boldsymbol{\tau}_{3,4}) \cdot (\hat{\mathbf{z}} \times \mathbf{p})$ where $\boldsymbol{\tau}_{1,2}$ and $\boldsymbol{\tau}_{3,4}$ represent the $SU(2)$ subalgebras in the spin subspaces spanned respectively by $\{|\frac{3}{2}\rangle, |\frac{1}{2}\rangle\}$ and $\{|-\frac{1}{2}\rangle, |-\frac{3}{2}\rangle\}$. The Hamiltonian is block-diagonalized since the spin components $|m_z > 0\rangle$ or $|m_z < 0\rangle$ are coupled separately. Therefore it can be decomposed into the superposition of two decoupled rank-1 SHEs in which the spin components $|\pm\frac{3}{2}\rangle$ flow in the same direction, opposite to that of $|\pm\frac{1}{2}\rangle$. Consequently, there is only a non-vanishing rank-2 spin tensor current with the spin tensor Hall conductivity $\sigma_{xy}^{zz} = q/2\pi$ (see Ref. [40] for details).

IX. DISCUSSION AND CONCLUSION

Besides the rank-2 spin tensor current \mathbf{J}_2^{zz} , we can similarly define other spin tensor currents like \mathbf{J}_2^{xy} or \mathbf{J}_2^z , and the corresponding spin tensor Hall conductivities usually vanish in the spin-1 model Eq. (5). However, we notice the following constraint:

$$\sigma_{xy}^{xx} + \sigma_{xy}^{yy} + \sigma_{xy}^{zz} = 0, \quad (14)$$

because $\sum_i N_{ii} = 0$ ($i = x, y, z$). According to the Kubo formula, we find $\sigma_{xy}^{xx} = 0$ and $\sigma_{xy}^{yy} = -q/8\pi$ which indeed satisfy Eq. (14). The rank-2 STHE does not require the spin components $|\pm 1\rangle$ to be necessarily superposed as $\frac{1}{\sqrt{2}}(|1\rangle + |-1\rangle)$. In principle, we can have a rank-2 spin tensor current arising from the counterflow of spin $|0\rangle$ and $\frac{1}{\sqrt{2}}(e^{i\alpha}|1\rangle + e^{i\beta}|-1\rangle)$ with arbitrary phases α and β . This extra phase degree of freedom can be induced by a generalized STMC under the gauge transformation $UH_{F=1}U^{-1}$ with $U = \text{diag}(e^{i\alpha}, 1, e^{i\beta})$, which also yields the universal rank-2 spin tensor Hall conductivity $\sigma_{xy}^{zz} = q/8\pi$ (see Ref. [40] for details). Moreover, there are other types of SOC, besides the discussed Rashba type $\boldsymbol{\tau}_T \cdot (\hat{\mathbf{z}} \times \mathbf{p})$, that can be used to realize the higher-rank STHE as well. For instance, we can consider the superposition of the Dresselhaus type SOCs in different spin subspaces as $\boldsymbol{\tau}_T \cdot \mathbf{p} + \boldsymbol{\tau}_V^* \cdot \mathbf{p}$ or even the mixture of the two different types as $\boldsymbol{\tau}_T \cdot (\hat{\mathbf{z}} \times \mathbf{p}) + \boldsymbol{\tau}_V^* \cdot \mathbf{p}$ that also leads to the rank-2 STHE with the universal rank-2 spin tensor Hall conductivity $\sigma_{xy}^{zz} = q/8\pi$.

In conclusion, we introduce and characterize the concept of universal STHE in large spin systems and propose its experimental realization with ultracold gases. The STHE can be used as a spin tensor filter to generate spin tensor cur-

rent that does not require the protection of TRS. Instead, the unique pseudo-TRS associated with the spin tensor paves the way to further quantize the STHE and realize a new kind of topological states protected by the pseudo-TRS. There are many physics remaining to be explored, such as the general construction of rank- n STHE for arbitrarily large spins, the effects of many-body interaction or disorder, the experimental realization in 2D solid-state materials with exotic spin-1 fermionic excitations [48], and the observation of STHE in the parameter space [27,38], etc. Our work defines a new class of SHEs and opens the door for manipulating the internal spin-tensor degrees of freedom, which can be used to design large-spin devices with new functionalities for spintronic applications.

ACKNOWLEDGMENTS

We thank Fan Zhang for helpful discussion. This work was supported by Air Force Office of Scientific Research (FA9550-20-1-0220), National Science Foundation (PHY-2110212, OMR-2228725), and Army Research Office (W911NF-17-1-0128).

-
- [1] J. E. Hirsch, Spin Hall Effect, *Phys. Rev. Lett.* **83**, 1834 (1999).
- [2] J. Sinova, S. O. Valenzuela, J. Wunderlich, C. H. Back, and T. Jungwirth, Spin Hall effects, *Rev. Mod. Phys.* **87**, 1213 (2015).
- [3] T. Seki, Y. Hasegawa, S. Mitani, S. Takahashi, H. Imamura, S. Maekawa, J. Nitta, and K. Takanashi, Giant spin Hall effect in perpendicularly spin-polarized FePt/Au devices, *Nat. Mater.* **7**, 125 (2008).
- [4] L. Liu, C.-F. Pai, Y. Li, H. W. Tseng, D. C. Ralph, R. A. Buhrman, Spin-torque switching with the giant spin hall effect of tantalum, *Science* **336**, 555 (2012).
- [5] Y. Niimi, Y. Kawanishi, D. H. Wei, C. Deranlot, H. X. Yang, M. Chshiev, T. Valet, A. Fert, and Y. Otani, Giant Spin Hall Effect Induced by Skew Scattering from Bismuth Impurities inside Thin Film CuBi Alloys, *Phys. Rev. Lett.* **109**, 156602 (2012).
- [6] E. Saitoh, M. Ueda, and H. Miyajima, Conversion of spin current into charge current at room temperature: Inverse spin-Hall effect, *Appl. Phys. Lett.* **88**, 182509 (2006).
- [7] T. Kimura, Y. Otani, T. Sato, S. Takahashi, and S. Maekawa, Room-Temperature Reversible Spin Hall Effect, *Phys. Rev. Lett.* **98**, 156601 (2007).
- [8] B. F. Miao, S. Y. Huang, D. Qu, and C. L. Chien, Inverse Spin Hall Effect in a Ferromagnetic Metal, *Phys. Rev. Lett.* **111**, 066602 (2013).
- [9] J.-C. Rojas-Sánchez, N. Reyren, P. Laczkowski, W. Savero, J.-P. Attané, C. Deranlot, M. Jamet, J.-M. George, L. Vila, and H. Jaffrès, Spin Pumping and Inverse Spin Hall Effect in Platinum: The Essential Role of Spin-Memory Loss at Metallic Interfaces, *Phys. Rev. Lett.* **112**, 106602 (2014).
- [10] M. Kimata, H. Chen, K. Kondou, S. Sugimoto, P. K. Muduli, M. Ikhlas, Y. Omori, T. Tomita, A. H. MacDonald, S. Nakatsuji, and Y. Otani, Magnetic and magnetic inverse spin Hall effects in a non-collinear antiferromagnet, *Nature (London)* **565**, 627 (2019).
- [11] C. L. Kane and E. J. Mele, Quantum Spin Hall Effect in Graphene, *Phys. Rev. Lett.* **95**, 226801 (2005).
- [12] B. A. Bernevig, T. L. Hughes, S.-C. Zhang, Quantum spin hall effect and topological phase transition in hgte quantum wells, *Science* **314**, 1757 (2006).
- [13] M. König, S. Wiedmann, C. Brune, A. Roth, H. Buhmann, L. W. Molenkamp, X.-L. Qi, S.-C. Zhang, Quantum spin hall insulator state in hgte quantum wells, *Science* **318**, 766 (2007).
- [14] Y. K. Kato, R. C. Myers, A. C. Gossard, D. D. Awschalom, Observation of the spin hall effect in semiconductors, *Science* **306**, 1910 (2004).
- [15] S. Murakami, N. Nagaosa, and S. C. Zhang, Dissipationless Quantum Spin Current at Room Temperature, *Science* **301**, 1348 (2003).
- [16] J. Sinova, D. Culcer, Q. Niu, N. A. Sinitsyn, T. Jungwirth, and A. H. MacDonald, Universal Intrinsic Spin Hall Effect, *Phys. Rev. Lett.* **92**, 126603 (2004).
- [17] Y. Kawaguchi and M. Ueda, Spinor Bose-Einstein condensates, *Phys. Rep.* **520**, 253 (2012).
- [18] E. Yukawa, M. Ueda, and K. Nemoto, Classification of spin-nematic squeezing in spin-1 collective atomic systems, *Phys. Rev. A* **88**, 033629 (2013).
- [19] B. Bradlyn, J. Cano, Z. Wang, M. G. Vergniory, C. Felser, R. J. Cava, B. Andrei Bernevig, Beyond Dirac and Weyl fermions: Unconventional quasiparticles in conventional crystals, *Science* **353**, aaf5037 (2016).
- [20] Z. M. Zhu, G. W. Winkler, Q. S. Wu, J. Li, and A. A. Soluyanov, Triple Point Topological Metals, *Phys. Rev. X* **6**, 031003 (2016).

- [21] P. Tang, Q. Zhou, and S.-C. Zhang, Multiple Types of Topological Fermions in Transition Metal Silicides, *Phys. Rev. Lett.* **119**, 206402 (2017).
- [22] H. Hu, J. Hou, F. Zhang, and C. Zhang, Topological Triply Degenerate Points Induced by Spin-Tensor-Momentum Couplings, *Phys. Rev. Lett.* **120**, 240401 (2018).
- [23] B. Q. Lv, Z.-L. Feng, Q.-N. Xu, X. Gao, J.-Z. Ma, L.-Y. Kong, P. Richard, Y.-B. Huang, V. N. Strocov, C. Fang, H.-M. Weng, Y.-G. Shi, T. Qian, and H. Ding, Observation of three-component fermions in the topological semimetal molybdenum phosphide, *Nature (London)* **546**, 627 (2017).
- [24] D. L. Campbell, R. M. Price, A. Putra, A. Valdés-Curiel, D. Trypogeorgos, and I. B. Spielman, Magnetic phases of spin-1 spin-orbit-coupled Bose gases, *Nat. Commun.* **7**, 10897 (2016).
- [25] X. Luo, L. Wu, J. Chen, Q. Guan, K. Gao, Z.-F. Xu, L. You and R. Wang, Tunable atomic spin-orbit coupling synthesized with a modulating gradient magnetic field, *Sci. Rep.* **6**, 18983 (2016).
- [26] T. Ollikainen, A. Blinova, M. Möttönen, and D. S. Hall, Decay of a Quantum Knot, *Phys. Rev. Lett.* **123**, 163003 (2019).
- [27] X. Tan, D.-W. Zhang, Q. Liu, G. Xue, H.-F. Yu, Y.-Q. Zhu, H. Yan, S.-L. Zhu, and Y. Yu, Topological Maxwell Metal Bands in a Superconducting Qutrit, *Phys. Rev. Lett.* **120**, 130503 (2018).
- [28] K. Sun, C. Qu, Y. Xu, Y. Zhang, and C. Zhang, Interacting spin-orbit-coupled spin-1 Bose-Einstein condensates, *Phys. Rev. A* **93**, 023615 (2016).
- [29] Z.-Q. Yu, Phase transitions and elementary excitations in spin-1 Bose gases with Raman-induced spin-orbit coupling, *Phys. Rev. A* **93**, 033648 (2016).
- [30] G. I. Martone, F. V. Pepe, P. Facchi, S. Pascazio, and S. Stringari, Tricriticalities and Quantum Phases in Spin-Orbit-Coupled Spin-1 Bose Gases, *Phys. Rev. Lett.* **117**, 125301 (2016).
- [31] X.-W. Luo, K. Sun, and C. Zhang, Spin-Tensor-Momentum-Coupled Bose-Einstein Condensates, *Phys. Rev. Lett.* **119**, 193001 (2017).
- [32] E. J. König and J. H. Pixley, Quantum Field Theory of Nematic Transitions in Spin-Orbit-Coupled Spin-1 Polar Bosons, *Phys. Rev. Lett.* **121**, 083402 (2018).
- [33] M. Naghiloo, M. Abbasi, Y. N. Joglekar, K. W. Murch, Quantum state tomography across the exceptional point in a single dissipative qubit, *Nat. Phys.* **15**, 1232 (2019).
- [34] I. Kuzmenko, T. Kuzmenko, Y. Avishai, and M. Sato, Spin-orbit coupling and topological states in an $F = \frac{2}{3}$ cold Fermi gas, *Phys. Rev. B* **98**, 165139 (2018).
- [35] J. Hou, H. Hu, C. Zhang, Topological phases in pseudospin-1 Fermi gases with two-dimensional spin-orbit coupling, *Phys. Rev. A* **101**, 053613 (2020).
- [36] G. Palumbo and N. Goldman, Revealing Tensor Monopoles through Quantum-Metric Measurements, *Phys. Rev. Lett.* **121**, 170401 (2018).
- [37] G. Palumbo and N. Goldman, Tensor Berry connections and their topological invariants, *Phys. Rev. B* **99**, 045154 (2019).
- [38] X. Tan, D.-W. Zhang, W. Zheng, X. Yang, S. Song, Z. Han, Y. Dong, Z. Wang, D. Lan, H. Yan, S.-L. Zhu, and Y. Yu, Experimental Observation of Tensor Monopoles with a Superconducting Qudit, *Phys. Rev. Lett.* **126**, 017702 (2021).
- [39] Z. Wu, L. Zhang, W. Sun, X.-T. Xu, B.-Z. Wang, S.-C. Ji, Y. Deng, S. Chen, X.-J. Liu, J.-W. Pan, Realization of two-dimensional spin-orbit coupling for Bose-Einstein condensates, *Science* **354**, 83 (2016).
- [40] See Supplemental Material <http://link.aps.org/supplemental/10.1103/PhysRevB.107.085410> for details about (S1) Gell-Mann matrices, SU(2) subalgebras, spin vectors and tensors, (S2) derivation of the rank-2 spin tensor Hall conductivity, (S3) pseudospin dynamics analysis, (S4) experimental realization of the spin-tensor-momentum coupling, (S5) 1D subbands due to transverse confinement, (S6) rank-2 spin tensor Hall effect for spin-3/2, and (S7) generalized spin-tensor-momentum coupling.
- [41] X.-J. Liu, K. T. Law, and T. K. Ng, Realization of 2D Spin-Orbit Interaction and Exotic Topological Orders in Cold Atoms, *Phys. Rev. Lett.* **112**, 086401 (2014).
- [42] R. N. Cahn, *Semi-Simple Lie Algebras and Their Representations* (Benjamin/Cummings, 1984).
- [43] G. Kimura, The Bloch vector for N-level systems, *Phys. Lett. A* **314**, 339 (2003).
- [44] L. H. Huang, Z. Meng, P. Wang, P. Peng, S.-L. Zhang, L. Chen, D. Li, Q. Zhou, and J. Zhang, Experimental realization of two-dimensional synthetic spin-orbit coupling in ultracold Fermi gases, *Nat. Phys.* **12**, 540 (2016).
- [45] Z. Meng, L. Huang, P. Peng, D. Li, L. Chen, Y. Xu, C. Zhang, P. Wang, and J. Zhang, Experimental Observation of a Topological Band Gap Opening in Ultracold Fermi Gases with Two-Dimensional Spin-Orbit Coupling, *Phys. Rev. Lett.* **117**, 235304 (2016).
- [46] S. Krinner, D. Stadler, D. Husmann, J.-P. Brantut, and T. Esslinger, Observation of quantized conductance in neutral matter, *Nature (London)* **517**, 64 (2015).
- [47] C.-C. Chien, S. Peotta, and M. Di Ventra, Quantum transport in ultracold atoms, *Nat. Phys.* **11**, 998 (2015).
- [48] S.-S. Wang, Y. Liu, Z.-M. Yu, X.-L. Sheng, L. Zhu, S. Guan, and S. A. Yang, Monolayer Mg₂C: Negative Poisson's ratio and unconventional two-dimensional emergent fermions, *Phys. Rev. Mater.* **2**, 104003 (2018).